Available online at www.sciencedirect.com
SCIENCE DIRECT
Polymer 47 (2006) 3073–3082
polymer
www.elsevier.com/locate/polymer

Effect of the degree of soft and hard segment ordering on the morphology and mechanical behavior of semicrystalline segmented polyurethanes

LaShanda T. James Korley [a,c], Brian D. Pate [b,c], Edwin L. Thomas [b,c], Paula T. Hammond [a,c,*]

[a] Department of Chemical Engineering, Massachusetts Institute of Technology, Cambridge, MA 02139, USA
[b] Department of Materials Science and Engineering, Massachusetts Institute of Technology, Cambridge, MA 02139, USA
[c] Institute for Soldier Nanotechnologies, Massachusetts Institute of Technology, Cambridge, MA 02139, USA

Received 2 December 2005; received in revised form 26 February 2006; accepted 27 February 2006

Abstract

The hierarchical microstructure responsible for the unique energy-absorbing properties of natural materials, like native spider silk and wood, motivated the development of segmented polyurethanes with soft segments containing multiple levels of order. As a first step in correlating the effects of crystallinity in the soft segment phase to the hard segment phase, we chose to examine the morphology and mechanical behavior of polyurethanes containing polyether soft blocks with varying tendencies to crystallize and phase segregate and the evolution of the microstructure with deformation. A series of high molecular weight polyurethanes containing poly(ethylene oxide) (PEO) (1000 and 4600 g/mol) and poly(ethylene oxide)–poly(propylene oxide)–poly(ethylene oxide) (PEO–PPO–PEO) (1900 g/mol) soft segments with varying hard segment content were synthesized using a two-step solution polymerization method. The presence of soft segment crystallinity (PEO 1000 g/mol) was shown to improve the storage modulus of the segmented polyurethanes below the T_m of the soft block and to enhance toughness compared to the PEO–PPO–PEO soft segment polyurethanes. We postulate that this enhancement in mechanical behavior is the result of crystalline soft regions that serve as an additional load-bearing component during deformation. Morphological characterization also revealed that the microstructure of the segmented polyurethanes shifts from soft segment continuous to interconnected and/or hard domain continuous with increasing hard segment size, resulting in diminished ultimate elongation, but enhanced initial moduli and tensile strengths. Tuning the soft segment phase crystallinity may ultimately lead to tougher polyurethane fibers.

Keywords: Segmented polyurethanes; Crystallinity; Toughness

1. Introduction

An examination of the molecular architecture of natural materials, such as spider silk, nacre, and collagen, has offered a new perspective on the development of materials with enhanced mechanical properties. Nacre, a natural composite, is arranged in a brick-and-mortar configuration with staggered layers of calcium carbonate (aragonite) platelets and a complex mixture of proteins [1–5] with ultimate mechanical properties superior to that of the individual components [6]. Anisotropic collagen fibrils are traversed by a layered arrangement of apatite mineral; the elastomeric collagen matrix provides a reinforcing effect within the hierarchical, core–shell morphology which influences the toughness of bone [7–10]. Native spider silk, a thermoplastic elastomer, consists of a majority matrix of alternating soft (amorphous, glycine-rich) with hard (β-pleated sheets of alanine) blocks [11–14]. The glycine-rich, continuous matrix also contains an 'oriented' amorphous component that is thought to play a key role in the extreme toughness of natural spider silk [12,15–17].

Thermoplastic elastomers, specifically multi-block copolymers such as segmented polyurethanes, provide a unique template for the design of synthetic materials with hierarchical microstructures. Here, we explore the influence of ordering within the continuous soft segment domain on material properties. Although many researchers have focused on the effect of soft segment (SS) type and length, hard segment (HS) type and length, hard domain crystallinity, and the extent of microphase segregation on structure–function relationships in segmented polyurethanes [18–23], only a few investigators have systematically targeted the role of soft domain ordering (both crystallization and orientation of non-crystalline soft

* Corresponding author. Address: Department of Materials Science and Engineering, Massachusetts Institute of Technology, Cambridge, MA 02139, USA. Tel.: +1 617 258 7577; fax: +1 617 258 5766.
E-mail address: hammond@mit.edu (P.T. Hammond).

0032-3861/$ - see front matter © 2006 Elsevier Ltd. All rights reserved.
doi:10.1016/j.polymer.2006.02.093

segment) on the morphological and mechanical behavior of segmented polyurethanes, particularly those containing highly crystalline hard domains. Kloss et al. studied the role of soft segment crystallinity for poly(caprolactone) (PCL)-based polyurethanes with amorphous hard domains, proposing a morphological model of PCL crystallites sequestered within the soft segment rich domain based on thermal analysis [24]. Skarja and Woodhouse analyzed a series of biodegradable polyurethane elastomers with varying PCL soft segment molecular weights. As the PCL soft segment crystallinity increased, these researchers suggested that the crystalline soft segment regions contributed to the overall reinforcement of the continuous domain, leading to enhanced mechanical behavior, including tensile strength, tensile modulus, and elongation-at-break [25]. Similar behavior has also been reported by Yen and Cheng upon increasing the crystalline poly(butylene adipate glycol) soft segment content in segmented polyurethanes [26]. Most recently, Sonnenschein et al. probed the enhancement of material properties using semicrystalline polyester diols as soft segments in low hard segment content polyurethanes, concluding that crystalline soft segments reinforce the hard phase according to a continuous reinforcement model [27].

Another way to alter the extent of order in the soft segment is to employ a side-chain LC soft segment. Nair et al. [28] modified a poly(siloxane) soft segment using liquid crystalline ordering groups. The deformation of these materials coupled the smectic A layers and the paracrystalline hard domains, suggesting that the incorporation of liquid crystalline moieties within the soft block may provide additional energy-absorbing mechanisms [29,30]. Yet, despite extensive studies of segmented copolymers, unanswered questions still exist. Specifically, we wish to address the interplay between hierarchical microstructure, deformation and mechanical function in materials with both high and low degrees of soft segment crystallinity.

We approach this study by developing polyurethane elastomers that incorporate several types of order within the soft phase. The soft segment is designed to contain a crystallizable segment, which is an additional load-bearing component and can undergo additional rearrangements during the deformation process. Poly(ethylene oxide) (PEO) and poly(ethylene oxide)–poly(propylene oxide)–poly(ethylene oxide) (PEO–PPO–PEO) were chosen as the crystallizable soft segments. While PEO-based polyurethane soft segments have been used in prior investigations [31–34], the focus of these studies has been primarily devoted to structural evolution and product development without an emphasis on systematic evaluation of property enhancement through soft domain ordering. The glass transition temperature of PEO is well below room temperature, but, depending on its molecular weight, the melting temperature may vary from 30 to 60 °C, which may moderate the modulus of the soft phase regions. PEO may also be copolymerized with an amorphous component, such as poly(propylene oxide) (PPO), to tune the degree of order exhibited within the soft domains.

2. Experimental

2.1. Materials

All materials were purchased from Sigma–Aldrich. Dibutyltin dilaurate (DBTDL) was stored under dried 0nitrogen and used as received. Anhydrous *N*,*N*′ -dimethylacetamide (DMAc), packaged in a sure/seal™ bottle, was used as received. The soft segments, (PEO) (1000 and 4600 g/mol) or (PEO–PPO–PEO) (1900 g/mol, 50 wt% PEO, each PEO block = 475 g/mol), were dehydrated and degassed under vacuum at 60 °C for 3–4 h and stored under dried nitrogen. The hard segment, 1,6-hexamethylene diisocyanate (HDI), was vacuum distilled and stored under dried nitrogen. The chain extender, 1,4-butanediol (BDO), was distilled under reduced pressure and stored under dried nitrogen. The hard segment content by weight was determined using the industry's standard, which overestimates the diisocyanate contribution to the hard domain, but provides direct comparison for commercially available materials:

$$\text{wt}(\%)\ \text{HS} = \frac{(n+1)M_{\text{HDI}} + nM_{\text{BDO}}}{(n+1)M_{\text{HDI}} + nM_{\text{BDO}} + M_{\text{SS}}}$$

n, moles of BDO; M_i, molecular weight.

2.2. Synthesis

The segmented polyurethanes were synthesized by means analogous to the synthetic procedure for PU-2-41, which is schematically depicted in Fig. 1. The polymerization was carried out in a glovebox to minimize side reactions with water. An excess amount of HDI (2.58 g, 15.3 mmol) was dissolved in 5 mL of DMAc, added to the three-neck flask, and stirred. PEO (5.12 g, 5.1 mmol) and five drops of DBTDL were dissolved in 25 mL of DMAc and added to an addition funnel fitted to a three-neck flask. The PEO/catalyst solution was slowly (~1 h) dripped into the HDI solution. The reaction mixture was then stirred at 65 °C for 3 h to form the pre-polymer.

The pre-polymer was then chain extended to form a high molecular weight polymer by adding BDO (0.923 g, 10.2 mmol) to the reaction mixture and stirring at 85 °C overnight; Fourier transform infrared spectroscopy (FT-IR) confirmed the disappearance of the isocyanate peak (2260 cm^{-1}). The reaction mixture was precipitated into a large excess of warm distilled water. The resulting polyurethane was washed with methanol and dried under vacuum until constant weight. All polyurethane samples were stored in amber bottles at 2–8 °C.

2.3. Gel permeation chromatography

Molecular weights and molecular weight distributions of soluble polymers were determined relative to polyethylene oxide standards using a Waters gel permeation chromatograph (GPC) equipped with two Styragel columns and RI detector with DMAc at 60 °C as the mobile phase.

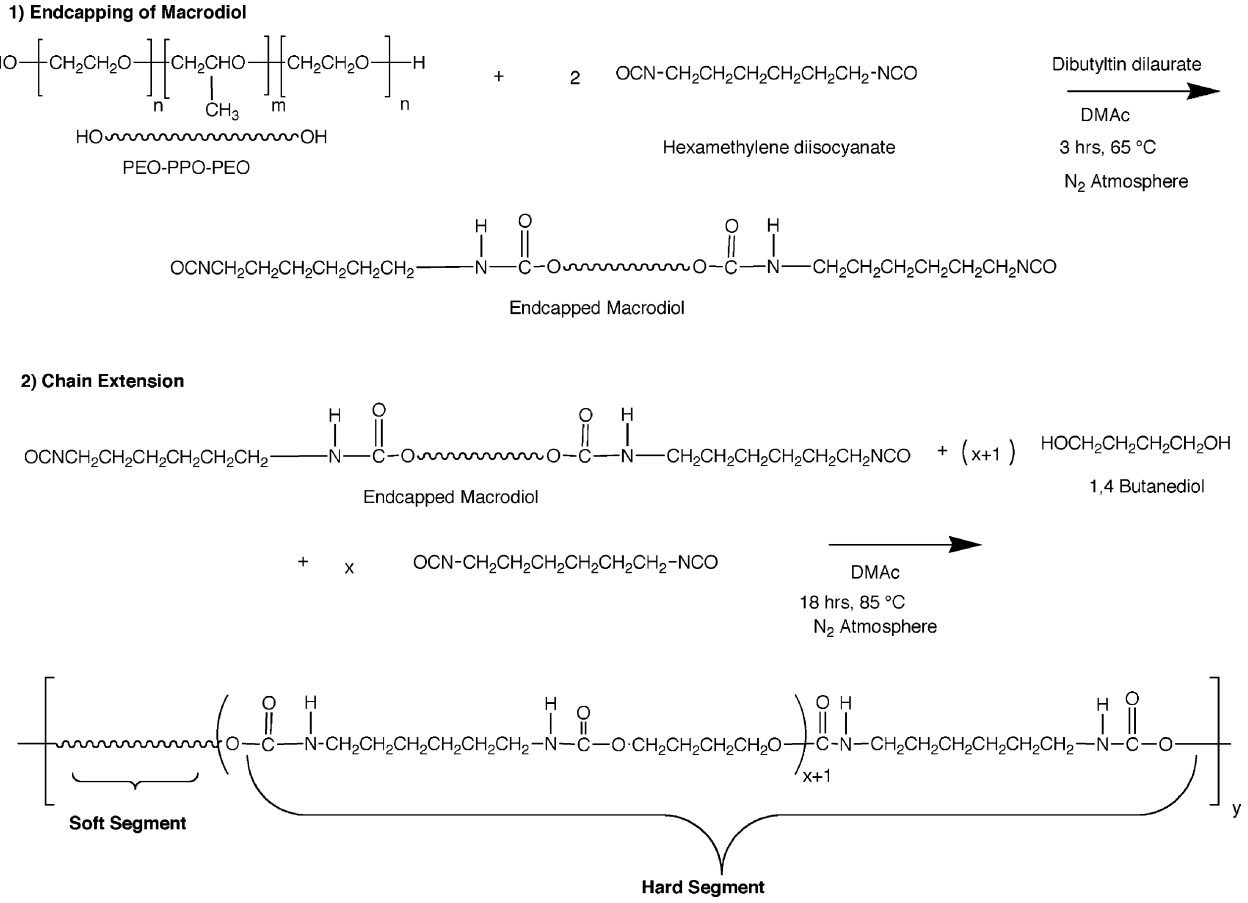

Fig. 1. Two-step solution synthetic route to high molecular weight segmented polyurethanes.

2.4. Fourier transform infrared spectroscopy

The polymerization was monitored by Fourier transform infrared spectroscopy (FT-IR) with a Thermo Nicolet Nexus 870 spectrometer using a DTGS KBr detector on West Georgia Laboratories poly(tetrafluoroethylene) (PTFE) IR cards.

2.5. Differential scanning calorimetry (DSC)

The thermal phase behavior of these thermoplastic polyurethanes was investigated using a TA Instruments Q1000 differential scanning calorimeter, operating at a heating and cooling rate of 10 °C/min under nitrogen atmosphere. As-precipitated, unannealed polymer samples were subjected to two heating and cooling cycles between −90 and 250 °C. The second heating cycle produced metastable morphologies of the polyurethanes. Transitions were recorded from the second heating and cooling scans using a linear extrapolation method (T_m) and the midpoint inflection method (T_g). DSC thermograms of annealed (60 °C, 1 h, vacuum) films yielded similar T_g, T_m, and heat of fusion data within instrumental error. The percent crystallinity within the soft block and the hard block was determined using a value of 197 J/g for the heat of fusion of PEO [35] and 84 J/g for the heat of fusion of HDI–BDO [36]. Since the pure soft segments used are less than 100% crystalline, percent crystallinity values reported are not absolute.

2.6. Small-angle and wide-angle X-ray scattering (SAXS and WAXS)

Small- and wide-angle X-ray scattering data was acquired at the X27C beamline at the National synchrotron light source (NSLS) at Brookhaven National Laboratory and at the G1 beamline at the Cornell high-energy synchrotron source (CHESS) using polyurethane samples prepared as thin films via solvent-casting from DMAc. The polyurethane thin films were annealed at 60 °C, which is above the glass transition of the hard and soft segment and the melting transition of the soft segment, for 1 h under vacuum to improve hard and soft domain segregation. The samples were cooled to room temperature in air. The X27C X-ray wavelength, λ, was 1.371 Å, monochromatized using a double-multilayer (silicon/tungsten) monochromator. The relative X-ray intensity was measured before (I_0) and after (I_1) the sample by using proportional counters. Further details of the X27C beamline are available at http://www.bnl.gov/nsls/x27c/. At the CHESS G1 beamline, $\lambda = 1.23$ Å, the beam was collimated to a horizontal divergence of 1 mrad via the wiggler 'K' factor and horizontal-focusing optics. Additional information regarding

the CHESS G1 beamline experimental set-up may be obtained at http://www.chess.cornell.edu/gline/index.htm.

Because the samples were isotropic (confirmed by polarizing optical microscropy), data were reduced from 2D (intensity vs. 2θ, χ) to 1D (intensity vs. 2θ) format by integrating over all values of χ, for each value of 2θ. Here, 2θ is the scattering angle and χ is the azimuthal angle. SAXS data have been expressed in terms of q, where $q=4\pi \sin(\theta)/\lambda$. The reduced data were normalized by I_1. A background pattern was collected for each sample environment, for a collection time equal to the sample collection time. A dark (blocked beam) pattern was measured for each collection time employed. The appropriate dark pattern was subtracted from each sample and background scattering pattern. Each sample pattern was then corrected using the following method:

$$\{\text{Corrected scattering pattern}\} = \{\text{sample pattern}\} - T(\{\text{background pattern}\})$$

T, the transmission ratio, was taken to be the ratio $I_1(\text{sample})/I_1(\text{background})$ where $I_1(x)$ was the measured beam intensity after the position of the sample or sample environment, as described above.

2.7. Atomic force microscopy (AFM)

A Nanoscope D3100 AFM with a Nanoscope IIIa controller and a multimode scanning probe microscope were used to probe the nanostructured morphology of these polyurethane films. Phase images of the sample surfaces were collected in tapping mode using Veeco NanoProbe tips (130 μm, 280–361 kHz).

2.8. Tensile testing

The tensile properties of these segmented polyurethanes were determined using a Zwick/Roell Z010 with a 500 N load cell and convex jaw grips with aluminum and flat polyurethane faces to minimize tearing at the grips. Polyurethane films were solvent-cast from 5 or 7.5 g/mL solutions in DMAc into Teflon molds and allowed to dry for ~3 days at room temperature. After 3 days, the films were annealed by vacuum drying at 60 °C for ~1 h prior to use and cooled to room temperature in air. The samples were elongated to failure at 100% of the initial gauge length per minute. Tensile properties were the average of at least three specimens.

2.9. Dynamic mechanical analysis (DMA)

DMA specimens were prepared as described in the tensile testing section above. The films were evaluated using a TA Instruments Q800 series DMA over a temperature range of −100–250 °C at a frequency of 1 Hz, a ramp rate of 3 °C min^{-1}, and an initial strain of ~0.2%.

3. Results and discussion

High molecular weight thermoplastic polyurethanes of varying soft segment content and type were synthesized by varying the stoichiometry of the macrodiol, chain extender, and diisocyanate. Table 1 details the soft segment type, molecular weight, and hard segment content (wt%) for these multi-block polymers. PEO-based polyurethanes with varying soft segment molecular weight were synthesized to study the effect of soft segment crystallinity on mechanical behavior. The segmented polyurethanes are classified according to the following structure: PU-*X*-*YY* where PU denotes polyurethane, *X* denotes the soft segment type (1 ≡ PEO–PPO–PEO 1900 g/mol, 2 ≡ PEO 1000 g/mol, 3 ≡ PEO 4600 g/mol), and *YY* denotes the hard segment content (wt%) (g BDO + g HDI)/(g soft segment + g BDO + g HDI). PU-3-33 was insoluble in available GPC eluents so molecular weight information is unavailable. However, PU-3-33 can be solubilized by refluxing in DMAc at 130 °C, making it possible to study some, but not all of the thermomechanical properties of this material. The pure hard segment polymer, HDI–BDO, was also synthesized for comparison.

3.1. Thermal characterization

Segmented polyurethanes generally display several thermal transitions, corresponding to the microstructure of the soft and hard domains. The soft segments undergo a low temperature glass transition, and, if semicrystalline, a melting transition; the hard segments may display a glass transition and/or multiple melting transitions. The soft segment glass transition and/or melting peak and the hard segment melting peak(s) of these polyurethanes with PEO and PEO–PPO–PEO soft segments were determined using DSC. Second heating data were used to compare the metastable morphologies of these as-precipitated samples. Similar thermal behavior was observed for the 1 h annealed film samples used in the X-ray analysis and mechanical studies. As shown in Table 2 and in Fig. 2, the soft segment glass transition of the PEO–PPO–PEO segmented

Table 1
Compositional details for PEO and PEO–PPO–PEO segmented polyurethanes

Polyurethane[a,b]	Soft segment	M_w (g/mol)	PDI	Hard segment content (wt%)
PU-1-26	PEO–PPO–PEO	84,100	1.7	26
PU-1-33	PEO–PPO–PEO	111,000	1.7	33
PU-1-43	PEO–PPO–PEO	68,700	1.8	43
PU-1-47	PEO–PPO–PEO	103,000	1.8	47
PU-2-41	PEO 1000	111,000	2.5	41
PU-3-33	PEO 4600	–	–	33
HDI–BDO	–	2600	1.1	100

[a] PU-*X*-*YY* where PU denotes polyurethane, *X* denotes the soft segment type (1 ≡ PEO–PPO–PEO 1900 g/mol, 2 ≡ PEO 1000 g/mol, 3 ≡ PEO 4600 g/mol), and *YY* denotes the hard segment size (wt%) (g BDO + g HDI)/(g soft segment + g BDO + g HDI).
[b] Pure hard segment.

Table 2
Thermal transitions and percent crystallinity of PEO and PEO–PPO–PEO segmented polyurethanes

	Soft segment				Hard segment		
	T_g[a] (°C)	T_m[b] (°C)	T_c[c] (°C)	ΔH_f[d], % crystallinity[e]	T_m[b] (°C)	T_c[c] (°C)	ΔH_f[d], % crystallinity[e]
PEO–PPO–PEO 1900	−69	17	−27	17, 9	–	–	–
PEO 1000	−56	37	18	154, 75	–	–	–
PEO 4600	−59	60	37	161, 77	–	–	–
PU-1-26	−62	–	–	–	140	95	48, 57
PU-1-33	−61	–	–	–	146	108	59, 70
PU-1-43	−62	–	–	–	153	119	64, 76
PU-1-47	−63	–	–	–	165	129	62, 74
PU-2-41	−50	11	−20	19, 10	132	98	43, 51
PU-3-33	−52	41	23	133, 68	165	109	35, 42
HDI–BDO	–	–	–	–	165	136	46

The thermal behavior of the pure soft segments (PEO and PEO–PPO–PEO) and hard segment (HDI–BDO) are also included.
[a] Glass transition temperature obtained from the second heating curve.
[b] Melting transition obtained from the second heating curve.
[c] Crystallization temperature obtained from the second cooling curve.
[d] Enthalpy of fusion values are per gram of soft segment and hard segment, respectively.
[e] Percent crystallinity $=((\Delta H_{f,\text{ HS or SS}})/(\Delta H_{f,\text{ pure HS or SS}}))\times 100$ (non-absolute).

polyurethanes is only slightly greater than for the pure PEO–PPO–PEO triblock ($T_g = -69$ °C) and is also independent of hard segment content (26–47 wt%), indicating a relatively small amount of hard segment mixing within the soft domain. Similar results were reported by Paik Sung et al. [37] in poly(tetramethylene oxide) soft segment polyurethanes and by O'Sickey et al. [38] for poly(propylene oxide) soft segments with a comparable hard segment range in 2,4-toluene diisocyanate (TDI)–ethylene diamine and MDI-mixed diamine HS polyurethanes, respectively. Similarly, the SS glass transition of PU-2-41 and PU-3-33 is only slightly increased from that of pure PEO 1000 and pure PEO 4600. These data are in contrast to MDI–PEO–PPO–PEO polyurethanes reported by Koberstein et al. [39], which exhibited significant phase mixing with MDI–BDO hard segments, especially as the percentage HS increased. For the PEO-based polyurethane series, the presence of soft segment crystallites must also be considered in the evaluation of the soft segment T_g since the mobility of the amorphous chains are restricted by neighboring crystallites [40]. While the soft segment glass transition temperature observed using DSC indicates the phase-separated microstructure of these segmented polyurethanes, DMA plots and AFM phase images along with the melting transition associated with hard domain ordering will provide further information regarding the phase-segregated morphology.

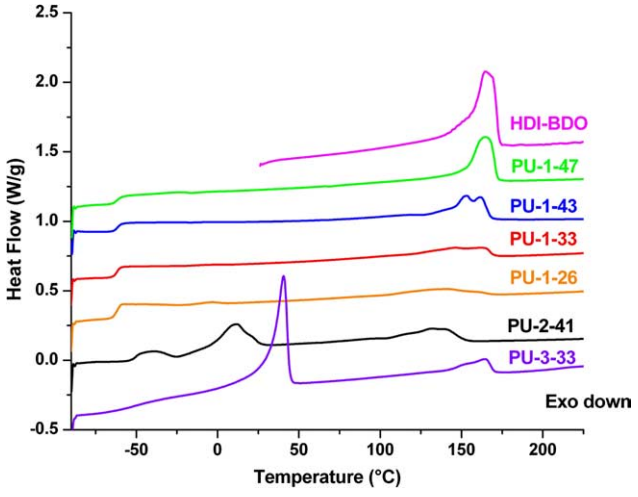

Fig. 2. Second heating DSC scans (10 °C min^{-1}) of as-precipitated segmented polyurethanes containing a PEO or PEO–PPO–PEO soft segment and a HDI–BDO hard segment and as-precipitated pure HDI–BDO. The *y*-axis was shifted for clarity.

The data in Table 2 indicate that the crystallinity of both the hard and soft segments is impacted by the soft segment composition. Although the pure PEO–PPO–PEO macrodiol has a melting transition at 17 °C, the PEO–PPO–PEO based polyurethanes do not exhibit any thermal transitions indicative of crystalline ordering within the soft domains; in these systems, crystallinity is hindered by the triblock composition and rather short PEO sequences. Soft segment crystallinity is, however, observed in the segmented polyurethanes containing PEO macrodiol soft segments, which are longer and not obstructed from ordering by the presence of a PPO central block. PU-2-41 shows a soft segment melting transition (11 °C, 19 J/g), which is significantly lower and weaker than the homopolymer PEO (1000 g/mol) melting peak as determined using DSC (37 °C). Thus, although PU-2-41 exhibits a soft segment T_m, these crystallites are relatively less stable and less organized than in the pure PEO homopolymer, as substantiated by its low percent SS crystallinity (10%). The higher molecular weight PEO soft segment (4600 g/mol) in PU-3-33 displays a more pronounced melting transition ($T_m = 41$ °C) and a higher soft segment percent crystallinity (68%) compared to PU-2-41, but this melting point is still depressed from the homopolymer PEO melting transition (60 °C). However, the percent soft segment crystallinity in PU-3-33 is comparable to the pure PEO 4600 (77%), which suggests that the longer PEO 4600 soft segment is able to more readily crystallize than the short PEO 1000 soft segment upon incorporation in the

polyurethane. Because DSC analysis suggests minimal phase-mixing between the hard and soft domains, the primary limitation to soft segment crystallization is domain confinement, inhibiting the growth of large, well-ordered soft segment crystallites [41–45]. This range of crystallinity within the soft segment, from non-crystalline PEO segments that might exhibit strain-induced ordering to partially crystalline segments (10 and 70%), allows comparisons of the properties of the resultant thermoplastic elastomers.

The as-precipitated pure hard segment, HDI–BDO, exhibits a melting transition at 165 °C (46 J/g) on the second heating cycle. MacKnight et al. [46] and Li et al. [36] reported values of 182 °C (70 J/g) and 180 °C (84 J/g), respectively, for pure HDI–BDO. Discrepancies between these literature values and our values are most likely due to variations in molecular weight and differences in thermal treatment by other researchers. Although not presented here, the 1st heating scans of the PEO and PEO–PPO–PEO polyurethanes display an annealing endotherm (53–86 °C) that shifts to higher temperatures as the hard segment composition increases, which has been associated with relaxation effects within the hard domains, specifically for MDI/BDO-based polyurethanes [47–49]. As expected, the hard-domain melting temperature increases as the hard segment content is increased, attaining a T_m of 165 °C at 47 wt% hard segment for the PEO–PPO–PEO soft segment polyurethanes that is equivalent to the pure hard domain due to the ability of longer HS sequences in the higher HS content polyurethane to form crystals.

The hard-domain melting transitions and enthalpies for the PEO–PPO–PEO soft segment based polyurethanes are higher than the pure PEO soft segment polyurethane at similar hard segment amounts. Comparison of PU-1-43 and PU-2-41, which both possess a similar hard segment percentage, but different soft segment length and type, indicate a 20 °C increase in hard domain melting point, and an increase of about 49% in the HS enthalpy of fusion. These observations may be the result of two effects. First, the longer soft segment (1900 vs. 1000 g/mol) generates larger domain sizes and decreases the amount of exposed hard segment surface area per unit volume in the continuous domain (for a given weight fraction HS), inducing a higher degree of phase separation [18]. Secondly, the PPO block in the PU-1-43 may enhance hard segment aggregation and microphase separation compared to PU-2-41, which contains PEO homopolymer as a soft segment. PEO, which has stronger hydrogen-bonding character, may induce less phase segregation. This interpretation is similar to Chang and Wilkes, who investigated the effect of the relative PPO vs. PEO content on the morphology of diamine-extended polyurethaneureas [50]. They reported that the PPO block promoted hard segment domain formation due to the hydrophobicity and incompatibility of PPO with the polar hard block. As the pure PEO soft segment molecular weight is increased from 1000 g/mol (PU-2-41) to 4600 g/mol (PU-3-33), we also expect stronger incompatibility between the hard and soft segment due to increased chain lengths, resulting in a higher degree of microphase separation and purer hard and soft domains. For example, consider PU-1-33 and PU-3-33, both materials exhibit a broad hard domain melting transition, but the melting peak of PU-3-33 is centered at that of the pure HDI–BDO (165 °C). Coupled with the significant crystallinity of the soft domain (T_m = 41 °C, 133 J/g), this observation implies that PU-3-33 is quite phase-segregated and contains both semicrystalline soft and semicrystalline hard domains. The broadness of the HS melting regime may be explained by the polydispersity of the hard segment sequence length. WAXS and preliminary SAXS (not shown) studies reinforce these observations [51].

The development of the hard segment melting transition as a function of hard segment content was also examined. At the lower hard segment percentages of these HDI–BDO polyurethanes (26–33%), a broad hard domain transition is observed. Increasing the hard segment content from 33 to 43% produces multiple melting endotherms, similar to the extensively studied MDI/BDO hard domain polyurethanes [23,49,52,53]. A further increase in the hard segment composition (47%) leads to a sharper hard segment melting transition, as shown in Fig. 2. The enthalpy of fusion values per gram of hard segment for these polyurethanes are tabulated in Table 2. The hard segment crystallinity increases as the hard segment composition is varied from 26 to 47%, which is also evidenced in the WAXS analysis.

3.2. Mechanical behavior

The elongation-at-break, toughness, ultimate tensile strength, and initial modulus were obtained from tensile measurements for these segmented polyurethanes and compared to a commercial polyurethane, as outlined in Table 3. At lower hard segment fractions, the hard segments aggregate to form hard domains, which serve as reinforcing fillers, in a soft segment matrix. As the hard segment composition increases, mechanical data are consistent with a shift in continuous domain morphology, producing materials with inter-connected hard domains, which is evidenced in the AFM phase images. As expected, these higher-hard segment content materials exhibit limited extensibility, but increased initial modulus, as shown in Table 3 and in Fig. 3.

What is most notable about the mechanical property data is the enhanced elongation at break and overall toughness of the PU-2-41 system in comparison with its PEO–PPO–PEO analogs, PU-1-43 and PU-1-47. The moduli of these polyurethanes are relatively similar, which suggests that the most important factor in initial modulus for these materials is

Table 3
Comparison of the tensile properties of annealed (60 °C; 1 h; vacuum) PEO and PEO–PPO–PEO soft segment polyurethanes and Elasthane®, a commercial PTMO–MDI–BDO segmented polyurethane

Sample	Elongation-at-break (%)	Ultimate tensile strength (MPa)	Initial modulus (MPa)	Toughness (MJ/m^3)
PU-1-26	587±67	14.9±1.2	72.5±3.7	65.1±9.0
PU-1-33	460±39	18.1±1.0	200±8.1	59.2±7.0
PU-1-43	447±76	23.6±1.2	156±15	77.4±14
PU-1-47	202±27	18.2±3.7	198±30	31.6±9.8
PU-2-41	711±24	35.6±0.31	209±7.3	148±5.4

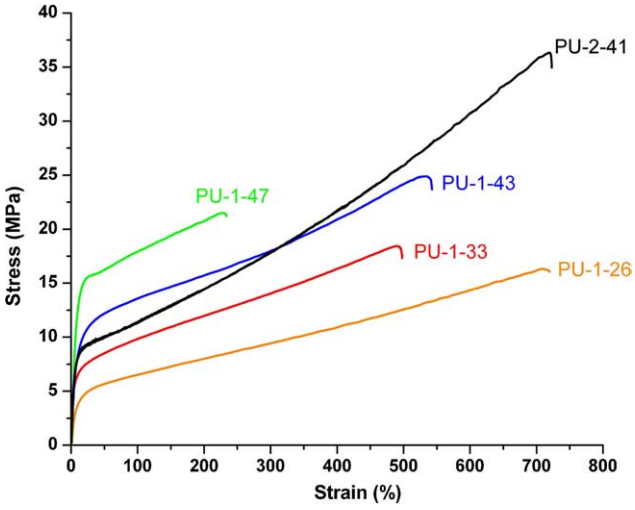

Fig. 3. Representative stress–strain behavior of annealed (60 °C; 1 h; vacuum) PEO and PEO–PPO–PEO soft segment polyurethanes.

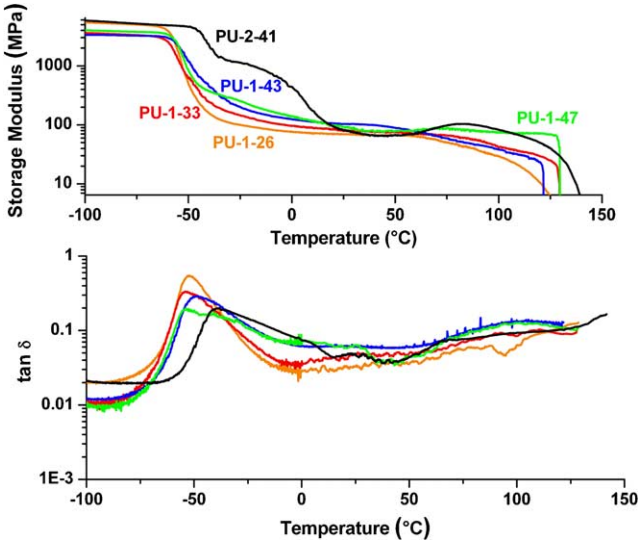

Fig. 4. Tan δ and storage modulus at 1 Hz of annealed (60 °C; 1 h; vacuum) PEO and PEO–PPO–PEO soft segment polyurethanes.

the hard segment content, as expected. However, it is not necessarily intuitive that the crystalline (i.e. PU-2-41) rather than amorphous polyether soft segment (i.e. PU-1-series) based polyurethanes were able to support much higher ultimate strains. Furthermore, based on the morphological studies described above, both types of SS systems were highly phase segregated, with enhanced phase segregation observed in the PPO containing polyurethanes; thus, these differences in mechanical properties are unlikely due to more defined segregated morphologies in the PU-2-41 case. PU-2-41 exhibits much higher energy absorption than the other materials, as indicated by its overall toughness.

One explanation for this enhanced extensibility and toughness is the presence of small PEO crystallites within the soft segment phase; these crystallites might act to absorb strain energy upon deformation through an unfolding of the crystalline lamellae or break up of crystalline segments. The semicrystalline SS matrix appears to serve as an effective stress-bearing phase during deformation without sacrificing extensibility. It is notable that the melting point of these crystallites is close to or just below room temperature; this may also be significant with respect to deformation mechanism. Even relatively low strains would be expected to induce strain-induced soft segment crystallization, but the low melt temperature also implies relatively high mobility of the soft segment chains, thus crystallites may be formed and deformed simultaneously throughout the deformation process. This form of transient, reformable order may play a role in toughening of the polymer matrix, much as is observed in a number of naturally occurring materials and as liquid crystalline order might be observed to do in other systems [54]. In fact, PU-2-41 displays superior ultimate mechanical properties compared to the PEO–PPO–PEO systems. The limited solubility of PU-3-33 prevented sufficient film formation of this material for tensile testing.

The dynamic mechanical behavior, illustrated in Fig. 4, of these segmented polyurethanes was also investigated. The soft segment crystallinity observed in PU-2-41 enhances the low-temperature stiffness of the polyurethane. As discussed, the crystalline regions of the soft domain serve as reinforcing fillers and contribute to the mechanical integrity of the polyurethane. Upon melting the PEO crystallites, hard domains support the microphase segregated morphology, as reflected by similar plateau moduli for PU-2-41 and PU-1-47.

The glass transition temperature of the soft segment is defined as the α transition in the Tan δ curve. tan δ was plotted as 40-point moving average values of the raw data. In the PEO–PPO–PEO soft segment polyurethanes, the tan δ peak broadens due to restrictions on the soft segment flexibility imposed by the hard domains, but no appreciable change in peak position is observed as the hard segment content increases. PU-2-41 also displays a broad and weaker tan δ transition, reflecting the retardation of molecular mobility from both the hard domains and the soft segment crystallites.

3.3. Morphological characterization

Morphological studies allow for further elucidation of the structural and thermal characteristics of these semicrystalline polyurethanes. Small-angle X-ray scattering data (not shown) reveal that the average spacing between hard domains in the phase-separated films containing 26–43 wt% hard segment is 12 nm. In the case of PU-1-47, however, the SAXS peak is shifted to $q = 0.58\ \mathrm{nm}^{-1}$, indicating a slightly smaller inter-domain spacing, d, of 11 nm. This correlates well with the AFM images (vide infra), which indicate a 'meshed' or more interconnected structure for PU-1-47 with decreased spacing between hard domains; this effect is due to the denser packing of hard domains within the matrix. The insensitivity of the hard domain periodicity to increasing hard segment content has been reported for a number of HDI–BDO polyurethanes; this behavior has been attributed to the chain-folding of the HS lamellar morphology [36].

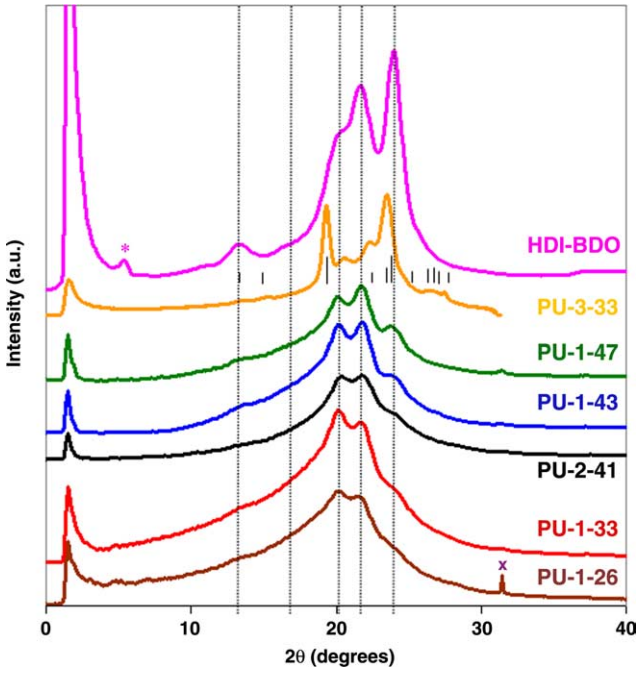

Fig. 5. Wide-angle X-ray scattering patterns of annealed (60 °C; 1 h; vacuum) polyurethane films (PU-1-26, PU-1-33, PU-1-43, PU-1-47, and PU-2-41) and as-precipitated pure hard segment and PU-3-33. The dashed vertical lines correspond to the HS spacings, while the hash marks on PU-3-33 indicate strong peaks of crystalline PEO. The peak marked with an asterisk is due to the Kapton support. The peak marked with an *x* is an impurity.

The wide-angle X-ray scattering data, presented in Fig. 5, for this series of segmented polyurethanes reveal a series of prominent peaks in the region $2\theta = 10$–$25°$. For all of the polymers except for PU-3-33, the Bragg spacings of the intensity maxima correlate well with the spacings we observe for a powder of the pure HDI–BDO HS, also presented in Fig. 5. However, the intensity distribution of the scattering profile varies continuously with the hard segment content. With decreasing hard segment, the intensity distribution becomes more dissimilar to that of crystalline HDI–BDO, and in particular the pattern becomes less resolved and the intensity of the peak at $d = 4.4$ Å increases relative to those at $d = 4.1$ and 3.7 Å. Fitting the pattern with a series of Voigt functions indicates that the scattering from the polymers with decreased hard segment possesses an increased contribution from a broad halo centered at $d = 4.2$ Å. We attribute this to the increased amorphous content of species with increasing percentage of PEO–PPO–PEO, or PEO of lower molecular weight (i.e. PU-2-41) [55]. This point will be elaborated further in an upcoming work devoted to an in-depth investigation of the scattering of these species. On the other hand, the scattering pattern of PU-3-33, which has as its soft segment PEO of higher molecular weight, bears a striking semblance to that of crystalline PEO. Indeed, by comparing the WAXS patterns of PEO 4600 macrodiol (not shown) and the PU-3-33 sample, it was determined that the dominant scattering peaks ($2\theta = 15.4$,

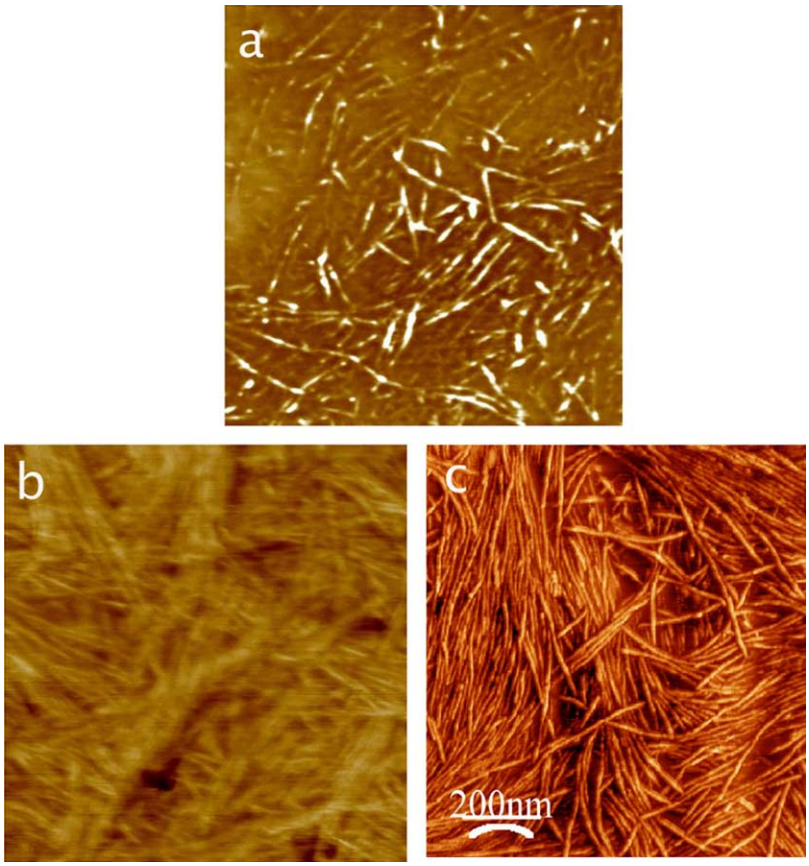

Fig. 6. AFM phase images of annealed (60 °C; 1 h; vacuum) of segmented polyurethane films: (a) PU-1-33, (b) PU-1-43, and (c) PU-1-47.

19.4, 22.5, 23.6 and 26.7) in PU-3-33 all arise from this more crystalline soft segment. In this case, the high degree of crystallinity within the soft block leads to scattering that almost completely masks the contribution from the less crystalline HDI–BDO hard domains.

AFM has been increasingly used as an alternative to transmission electron microscopy (TEM) for the visual interpretation of the nanostructure of segmented polyurethanes [56–58]. The surface morphology of these multi-block polyurethanes was imaged using tapping mode AFM. Fig. 6 illustrates the morphologies of these materials. The high modulus hard domains and the non-crystalline, low modulus soft blocks appear as light and dark regions, respectively, in these phase contrast images. At lower hard segment contents, the hard domains are randomly dispersed in a continuous soft domain, which is reflected in larger average inter-domain spacings. As the hard block length increases, in interlocking hard segment morphology develops, decreasing the average distance between hard domains, but increasing the thickness of the hard domain, which is confirmed by the SAXS studies. The development of a hard domain-continuous morphology upon increasing the hard segment size has been observed in other segmented polyurethanes [18,56]. The influence of this shift from a continuous, soft matrix to a hard, interlocking morphology directly influences the mechanical behavior of these multi-block polyurethanes. Unfortunately, both PEO soft segment polyurethanes displayed extremely rough surfaces, limiting their resolution via AFM.

4. Conclusions

A series of high molecular weight polyurethanes containing PEO–PPO–PEO and PEO soft segment and HDI–BDO hard segments were developed to examine the relative roles of hierarchical order via hard and soft segment crystallinity in polyurethanes. The PEO–PPO–PEO soft segments did not exhibit crystallinity when incorporated into polyurethanes; however, PEO soft segments were semicrystalline. An increase in the PEO soft segment molecular weight contributed to increased incompatibility between the hard and soft domains due to molecular weight. As the hard segment content was increased, an enhancement in hard domain crystallinity was observed using several thermal, X-ray, and AFM techniques. The inter-hard domain spacing decreased slightly with increasing hard segment in the PEO–PPO–PEO and PEO 1000 polyurethanes. A lamellar or rod-like morphology was assigned to these PEO-containing polyurethanes.

Although in general, when hard segment content was increased, the ultimate elongation decreased and the initial moduli and tensile strength increased, the presence of soft segment crystallites actually reinforced the polyurethane matrix in PU-2-41. The introduction of deformable SS crystals within the continuous matrix of segmented polyurethanes offers an additional method of designing higher performance materials. In these hierarchical materials, the soft segments not only impart extensibility, but the ordered SS regions also reinforce the polyurethane matrix during the deformation process in a similar manner to the hard domains, dissipating energy and contributing to the overall toughness. Investigation of material systems with multiple levels of order within the continuous matrix may further direct the development of moderate strain, high modulus fiber-forming materials.

Acknowledgements

This research was supported by, the US Army through the Institute for Soldier Nanotechnologies, under Contract DAAD-19-02-0002 with the US Army Research Office. This work is based upon research conducted at the Cornell High Energy Synchrotron Source (CHESS), which is supported by the National Science Foundation and the National Institutes of Health/National Institute of General Medical Sciences under award DMR-0225180. Research carried out (in whole or in part) at the National Synchrotron Light Source, Brookhaven National Laboratory, which is supported by the US Department of Energy, Division of Materials Sciences and Division of Chemical Sciences, under Contract No. DE-AC02-98CH10886. This work made use of MRSEC Shared Experimental Facilities at MIT, supported by the National Science Foundation under award number DMR-02-13282. L. James Korley gratefully acknowledges Lucent Corporation for a Cooperative Research Fellowship and Ford Motor Company for an MIT Ford Motor Company Fellowship.

References

[1] Neves NM, Mano JF. Mater Sci Eng 2005;C25(2):113–8.
[2] Weiner S, Addadi L. J Mater Chem 1997;7(5):689–702.
[3] Weiner S, Addadi L, Wagner HD. Mater Sci Eng 2000;C11(1):1–8.
[4] Checa AG, Rodriguez-Navarro AB. Biomaterials 2005;26(9):1071–9.
[5] Towe KM, Hamilton GH. Calcified Tissue Res 1967;1:306–18.
[6] Ji B, Gao H. J Mech Phys Solids 2004;52(9):1963–90.
[7] Gutsmann T, Fantner GE, Venturoni M, Ekani-Nkodo A, Thompson JB, Kindt JH, et al. Biophys J 2003;84(4):2593–8.
[8] Zioupos P, Currey JD, Hamer AJ. J Biomed Mater Res 1999;45(2):108–16.
[9] Sarkar SK, Hiyama Y, Niu CH, Young PE, Gerig JT, Torchia DA. Biochemistry 1987;26(21):6793–800.
[10] Thompson JB, Kindt JH, Drake B, Hansma HG, Morse DE, Hansma PK. Nature 2001;414(6865):773–6.
[11] Gosline JM, Guerette PA, Ortlepp CS, Savage KN. J Exp Biol 1999;202(23):3295–303.
[12] Grubb DT, Jelinski LW. Macromolecules 1997;30(10):2860–7.
[13] O'Brien JP, Fahnestock SR, Termonia Y, Gardner KCH. Adv Mater 1998;10(15):1185–95.
[14] Xu M, Lewis RV. Proc Natl Acad Sci USA 1990;87(18):7120–4.
[15] Grubb DT, Ji GD. Int J Biol Macromol 1999;24(2–3):203–10.
[16] Simmons A, Ray E, Jelinski LW. Macromolecules 1994;27(18):5235–7.
[17] Simmons AH, Michal CA, Jelinski LW. Science 1996;271(5245):84–7.
[18] Abouzahr S, Wilkes GL, Ophir Z. Polymer 1982;23(7):1077–86.
[19] Briber RM, Thomas EL. J Macromol Sci, Phys Ed 1983;B22(4):509–28.
[20] Briber RM, Thomas EL. J Polym Sci, Part B: Polym Phys 1985;23(9):1915–32.
[21] Christenson CP, Harthcock MA, Meadows MD, Spell HL, Howard W, Creswick MW, et al. J Polym Sci, Part B: Polym Phys 1986;24(7):1401–39.
[22] Kimura I, Ishihara H, Ono H, Yoshihara N, Nomura S, Kawai H. Macromolecules 1974;7(3):355–63.

[23] Koberstein JT, Galambos AF. Macromolecules 1992;25(21):5618–24.
[24] Kloss J, Munaro M, De Souza GP, Gulmine JV, Wang SH, Zawadzki S, et al. J Polym Sci, Part A: Polym Chem 2002;40(23):4117–30.
[25] Skarja GA, Woodhouse KA. J Appl Polym Sci 2000;75(12):1522–34.
[26] Yen MS, Cheng KL. J Appl Polym Sci 1994;52(12):1707.
[27] Sonnenschein MF, Lysenko Z, Brune DA, Wendt BL, Schrock AK. Polymer 2005;46(23):10158–66.
[28] Nair B, Osbourne MAR, Hammond PT. Macromolecules 1998;31(25): 8749–56.
[29] Nair BR, Gregoriou VG, Hammond PT. Polymer 2000;41(8):2961–70.
[30] Nair BR, Gregoriou VG, Hammond PT. J Phys Chem B 2000;104(33): 7874–80.
[31] Chang AL, Briber RM, Thomas EL, Zdrahala RJ, Critchfield FE. Polymer 1982;23:1060–8.
[32] Lan PN, Corneillie S, Schacht E, Davies M, Shard A. Biomaterials 1996; 17(23):2273–80.
[33] Lee D, Lee S-H, Kim S, Char K, Park JH, Bae YH. J Polym Sci, Part B: Polym Phys 2003;41:2365–74.
[34] Mao C-L. In: States U, editor. Thermoplastic polyurethane elastomer. US: Uniroyal, Inc.; 1978.
[35] Brandrup J, Immergut EH, Grulke EA, editors. Polymer handbook. Hoboken, NJ: Wiley; 1999.
[36] Li YJ, Ren ZY, Zhao M, Yang HC, Chu B. Macromolecules 1993;26(4): 612–22.
[37] Paik Sung CS, Hu CB, Wu CS. Macromolecules 1980;13(1):111–6.
[38] O'Sickey MJ, Lawrey BD, Wilkes GL. J Appl Polym Sci 2002;84(2): 229–43.
[39] Koberstein JT, Galambos AF, Leung LM. Macromolecules 1992;25(23): 6195–204.
[40] Garrett JT, Xu R, Cho J, Runt J. Polymer 2003;44(9):2711–9.
[41] Gogolewski S. Colloid Polym Sci 1989;267(9):757–85.
[42] Loo Y-L, Register RA, Ryan AJ, Dee GT. Macromolecules 2001;34(26): 8968–77.
[43] Loo Y-L, Register RA, Ryan AJ. Macromolecules 2002;35(17): 2365–74.
[44] Lee L-B, Register RA. Macromolecules 2004;37(19):7278–84.
[45] Johnson MA, Iyer J, Hammond PT. Macromolecules 2004;37(7): 2490–501.
[46] Kajiyama T, MacKnight WJ. Polym J 1970;1:548.
[47] Chen KC, Sheieh TS, Chul JYM. Macromolecules 1998;31:1312.
[48] Van Bogart JWC, Bluemeke DA, Cooper SL. Polymer 1981;22:1428.
[49] Saiani A, Daunch WA, Verbeke H, Leenslag JW, Higgins JS. Macromolecules 2001;34(26):9059–68.
[50] Chang Y-JP, Wilkes GL. J Polym Sci, Polym Phys Ed 1975;13:455–76.
[51] James-Korley LT. PhD Thesis. Cambridge, MA: Massachusetts Institute of Technology; 2005.
[52] Van Bogart JWC, Gibson PE, Cooper SL. J Polym Sci, Part B: Polym Phys 1983;21(1):65–95.
[53] Saiani A, Rochas C, Eeckhaut G, Daunch WA, Leenslag JW, Higgins JS. Macromolecules 2004;37(4):1411–21.
[54] Li J, Tammer M, Kremer F, Komp A, Finkelmann H. Eur Phys J E 2005; 17(4):423–8.
[55] Thompson P, Cox DE, Hastings JB. J Appl Crystallogr 1987;20:79–83.
[56] Aneja A, Wilkes GL. Polymer 2003;44(23):7221–8.
[57] Chen X, Roberts CJ, Zhang J, Davies MC, Tendler SJB. Surf Sci 2002; 519(1–2):L593–L8.
[58] McLean RS, Sauer BB. Macromolecules 1997;30(26):8314–7.